nature electronics

ARTICLES

https://doi.org/10.1038/s41928-020-0414-z

Non-reciprocal transmission of microwave acoustic waves in nonlinear parity–time symmetric resonators

Linbo Shao[1]✉, Wenbo Mao[1,2], Smarak Maity[1], Neil Sinclair[1,3], Yaowen Hu[1], Lan Yang[2] and Marko Lončar[1]✉

Acoustic waves are versatile on-chip information carriers that can be used in applications such as microwave filters and transducers. Nonreciprocal devices, in which the transmission of waves is non-symmetric between two ports, are desirable for the manipulation and routing of phonons, but building acoustic non-reciprocal devices is difficult because acoustic systems typically have a linear response. Here, we report non-reciprocal transmission of microwave surface acoustic waves using a nonlinear parity–time symmetric system based on two coupled acoustic resonators in a lithium niobate platform. Owing to the strong piezoelectricity of lithium niobate, we can tune the gain, loss and nonlinearity of the system using electric circuitry. Our approach can achieve 10 dB of non-reciprocal transmission for surface acoustic waves at a frequency of 200 MHz, and we use it to demonstrate a one-way circulation of acoustic waves in cascading non-reciprocal devices.

Acoustic devices operating at microwave frequencies have recently been integrated into solid-state platforms[1–6]. Surface acoustic waves (SAWs)[7]—elastic waves that propagate along the surfaces of solid materials—have, in particular, been proposed as an interface for solid-state quantum systems, including superconducting qubits[1,2], defect centres[3,4] and nanomechanical oscillators[5]. In such systems, continuously operating, non-magnetic non-reciprocal devices are desired for phonon isolation and networking. Non-reciprocal acoustic devices are based on a broken time-reversal symmetry and can exhibit one-way transmission of propagating waves. Such asymmetric acoustic wave transmission has been demonstrated in bulk media with circulating fluids[8], superlattices with nonlinear media[9,10], macroscopic metamaterials[11,12], a water-submerged phononic crystal[13] and in deformed water–air interfaces via the acoustic radiation pressure effect[14]. However, these approaches are limited to operating frequencies below a few megahertz. Non-reciprocity at microwave frequencies has been demonstrated with SAWs in ferromagnetic materials, but only weak phonon isolation was achieved[15,16]. Moreover, ferromagnetic devices require magnetic fields, making them incompatible with many solid-state systems, including superconductors and electron spins. Non-reciprocal phonon transmission using optomechanics has also recently been explored[17], but the approach remains experimentally challenging, especially for integrated platforms.

Parity–time (PT) symmetric systems[18–21] consist of coupled non-Hermitian subsystems with balanced gain and loss configurations, and have been explored in integrated optical[22–29], acoustic[30–36] and electrical[37] platforms. In particular, acoustic PT systems have been used for wave detection and manipulation, including non-reciprocal wave transmission. Loudspeakers loaded with tailored electrical circuits[30,31] or an airflow duct[32] have enabled PT systems for airborne acoustic waves and demonstrated asymmetric sensing and unidirectional invisibility[33]. Acoustic PT systems could also be constructed by optomechanical systems[35].

In this Article, we report a PT-symmetric SAW system that operates at frequencies of hundreds of megahertz. The system is based on two coupled resonators in a lithium niobate ($LiNbO_3$) platform. To introduce acoustic gain, loss and nonlinearity, we rely on the fact that SAWs in a piezoelectric material (such as $LiNbO_3$) are not purely elastic waves but also have an electric field component. In particular, we show that the gain in the SAW resonator can introduce strong nonlinearity and be tuned electrically to fully compensate for the loss of the resonator. Furthermore, we vary the coupling strength, gain and loss of the resonators to break the PT symmetry of the system and show non-reciprocal transmission of the acoustic waves. To illustrate the potential of our approach, we also demonstrate a one-way SAW circulation using two non-reciprocal devices connected in series.

PT-symmetric SAW resonators

Our PT-symmetric SAW system consists of two coupled SAW resonators, defined by Bragg mirrors. Each resonator contains distributed cross-finger electrodes, known as interdigital transducers (IDTs), which are connected to external electronic circuits to provide gain and loss (Fig. 1a,b). SAWs propagate along the crystalline X direction on the surface of 128° Y-cut $LiNbO_3$, and this configuration provides strong electromechanical coupling and low propagation loss[38]. The Bragg mirrors feature >30 dB reflectivity at a frequency of 200 MHz, over a bandwidth of 8 MHz (Fig. 1c), and are fabricated by etching grooves into $LiNbO_3$ with a pitch of 10 μm to match the acoustic half-wavelength[39]. Within the reflection band of the Bragg mirror, a SAW resonator without the IDT exhibits three resonant modes with intrinsic quality factors of up to 10^4. Two more IDTs, situated outside the coupled resonator system, are used as an emitter–receiver pair for transmission measurements. These IDTs are designed to have bandwidths larger than the Bragg reflection band, and their transmission of −14 dB (Fig. 1c) is excluded in the

[1]John A. Paulson School of Engineering and Applied Sciences, Harvard University, Cambridge, MA, USA. [2]Department of Electrical and Systems Engineering, Washington Univerity, St Louis, MO, USA. [3]Division of Physics, Mathematics and Astronomy, and Alliance for Quantum Technologies (AQT), California Institute of Technology, Pasadena, CA, USA. ✉e-mail: shaolb@seas.harvard.edu; loncar@seas.harvard.edu

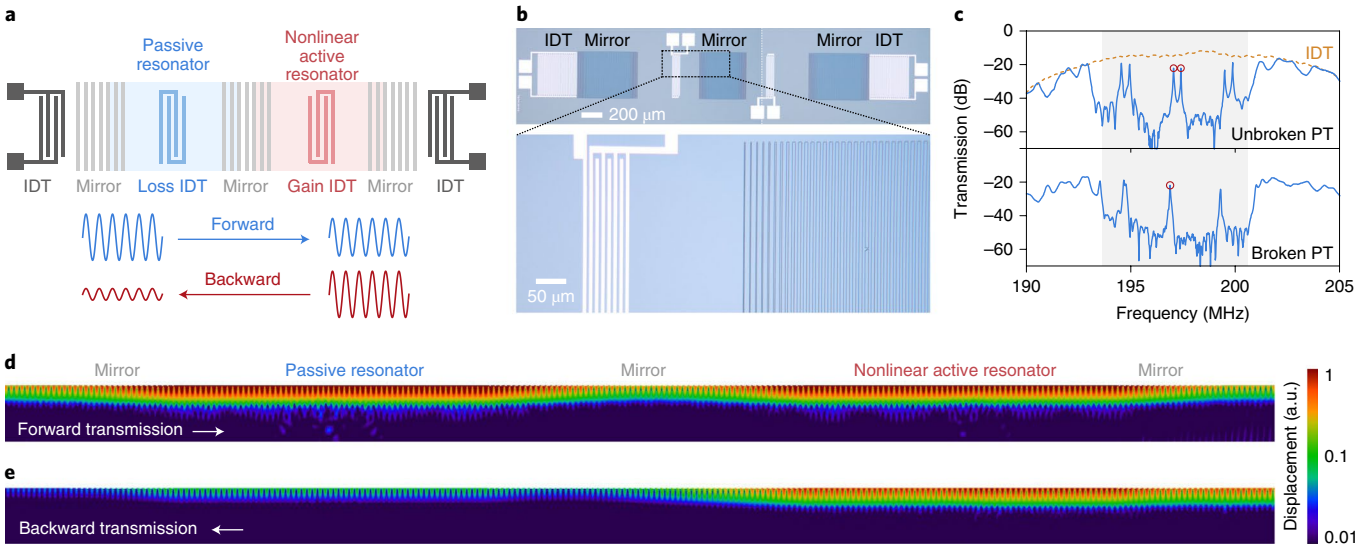

Fig. 1 | Non-reciprocal SAW transmission using nonlinear PT-symmetric resonators. a, Schematic of our coupled SAW resonator system for non-reciprocal transmission. Loss and gain are introduced in the passive and active resonators, respectively. IDTs are used to create gain and loss and to generate and receive SAWs. For devices in the broken PT-symmetric regime, higher transmission is expected in the forward direction than the backward direction. **b**, Microscope images of our fabricated device. The dark and bright areas are grooves etched into the $LiNbO_3$ surface and aluminium electrodes, respectively. The large square aluminium pads are used to connect to external circuits by wire bonding. The white dashed line in the top image indicates the stitching boundary between two optical fields used to image the device. **c**, Measured transmission spectra of one device with strong coupling in the unbroken PT-symmetric (reciprocal) regime and another device with weak coupling in the broken PT-symmetric (non-reciprocal) regime. Resonances are observed in the bandgap (shaded grey) of a SAW Bragg mirror. For the coupled modes of interest (red circles), a mode splitting is observed in the unbroken PT-symmetric regime, while only a single resonance is observed in the broken PT-symmetric regime. The transmission spectrum of a pair of IDTs is also plotted. **d**,**e**, Numerical simulations of the magnitude of elastic displacement due to SAWs propagating through broken PT-symmetric (non-reciprocal) resonators in the forward (**d**) and backward (**e**) directions. The plots are stretched in the vertical direction for clarity.

characterization of our PT-symmetric resonators. We refer to the resonator with gain (loss) as the active (passive) resonator, and we consider the forward direction of propagation to be from the passive to the active resonator (Fig. 1a).

In a PT-symmetric system, there are two distinct regions of the parameter space, determined by a coupling strength μ between the resonators and their gain $g>0$ and loss $\gamma<0$ (ref. [36]). In the unbroken PT-symmetric regime, $\mu>(g+|\gamma|)/2$. The real parts of the eigenvalues of the system are different, resulting in a mode splitting of the observed transmission spectrum (Fig. 1c). The transmission is reciprocal in this regime. In the broken PT-symmetric regime, the coupling between two resonators is weak, $\mu<(g+|\gamma|)/2$, and the eigenvalues share identical real parts. This corresponds to a single resonance peak in the transmission spectrum, as we observe experimentally in Fig. 1c. In the presence of additional nonlinearities, the unequal localization in the active resonator between the forward and backward inputs can result in non-reciprocal transmission[23,34]. The details of our acoustic PT-symmetric system are discussed in Supplementary Note 1.

We numerically evaluated the non-reciprocal response of the coupled resonator system with an 80-groove Bragg mirror between the resonators (Fig. 1d,e). In this case, the weak coupling between the resonators puts the system in the broken PT-symmetric regime. The energy flow between the two resonators is too small to reach equilibrium. As a result, the forward-propagating wave (Fig. 1d) is first attenuated in the passive resonator, before entering the active resonator featuring nonlinear gain. Thus, the wave experiences the high-gain regime of the nonlinear active resonator, the signal is amplified, and the overall system transmission is high. On the other hand, the backward-propagating wave (Fig. 1e) first enters the nonlinear active resonator. Due to its high amplitude, the wave experiences lower gain due to gain saturation. Next, it enters the passive resonator, where it experiences loss before it is detected via the IDT, resulting in a low transmission. The PT symmetry breaking induces a stronger localization in the active resonator for the backward-propagating wave than the forward wave. The stronger localization results in a lower gain and leads to a non-reciprocal transmission. On the other hand, the use of a 30-groove Bragg mirror between the two resonators yields stronger coupling than with the 80-groove mirror, putting the system in the unbroken PT-symmetric regime. Here, an equilibrium between the two resonators is reached, resulting in similar SAW amplitudes in the active and passive resonators. Thus, the transmission spectra for backward and forward-propagating SAWs are reciprocal (Supplementary Note 4).

In our experiment, we first used a single resonator geometry to characterize the SAW gain and nonlinearity from an additional IDT inserted in the middle of the resonator and connected to a variable-gain electronic circuit (Fig. 2a). Specifically, the IDT was connected (using wire bonding) to a negative-resistance electric circuit implemented by an operational amplifier with feedback resistors (Fig. 2b). The trimmer resistor R_f in Fig. 2b tunes the effective negative resistance of the circuit (for details see Supplementary Note 5). Instead of dissipating electric energy, a negative resistor circuit outputs electric energy with an applied voltage, and thus provides the gain for SAWs (via the piezoelectric effect). Owing to the presence of gain and noise in the resonator, a SAW can be detected via the receiving IDT without input. Below a certain gain threshold, the spectrum of the output SAW features a resonance linewidth of 94(1) kHz, which is determined by the loss of the resonator. Detailed transmission measurements were performed in this regime to characterize the SAW amplification process (Supplementary Fig. 10). When the gain is increased, SAW self-oscillation occurs and the linewidth of the output SAW narrows significantly (Fig. 2c). This indicates that the gain can fully compensate for the loss of the SAW

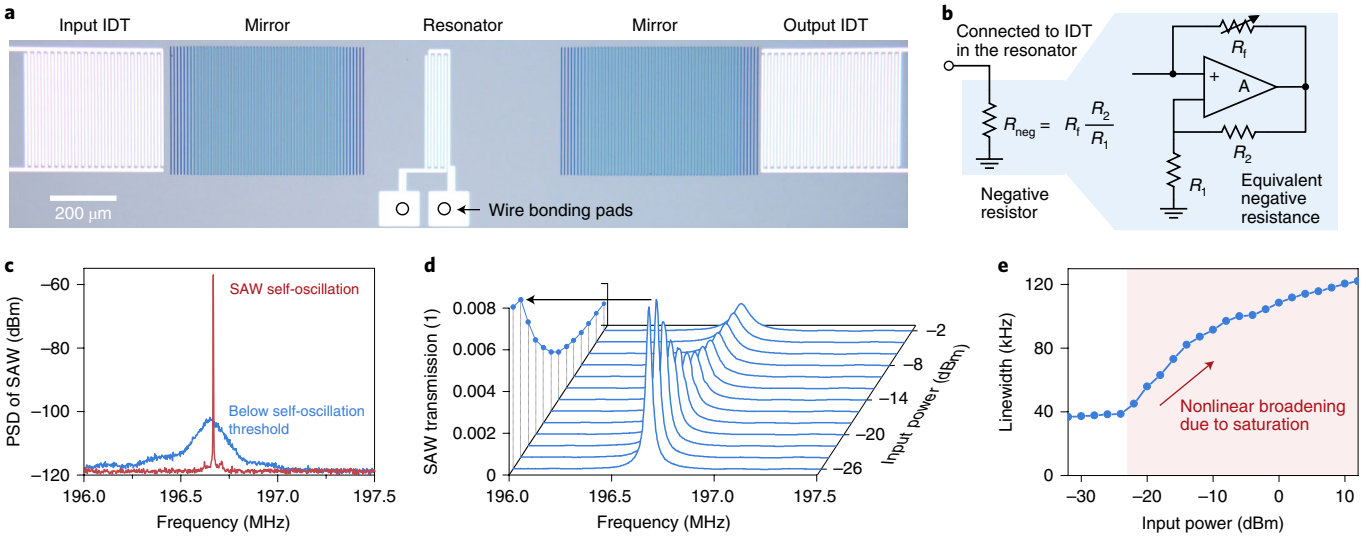

Fig. 2 | Characterization of SAW gain and nonlinearity. a, Microscope image of a single SAW resonator for gain and nonlinearity characterization. The gain for the SAWs is provided by the interdigital electrodes connected to an electronic circuit by wire bonding. **b**, Electronic diagrams of the negative resistor providing SAW gain. The negative resistance is implemented by an operational amplifier and resistors. The equivalent negative resistance is tuned using the adjustable resistor R_f. **c**, Measured power spectral density (PSD) of the output SAW from the active resonator. When the gain is below the threshold for self-oscillation, the spectrum of the SAW collected at the output IDT shows resonance with a linewidth of 94(1) kHz determined by the quality factor of the resonator ($Q = 2{,}000$). When the gain is increased above the threshold, the resonator linewidth narrows below 2.5 kHz (the spectral resolution set by the spectrum analyser) and SAW self-oscillation is observed. **d**,**e**, Transmission spectra (**d**) and linewidth (**e**) of the nonlinear active resonator for various SAW input powers. The transmission resonance broadens, and its amplitude reduces for greater input powers due to the nonlinear saturation.

resonator. Importantly, our negative resistance circuit features nonlinear gain. For a high input signal, the operational amplifier operates in the saturation regime, in which its output voltage is clamped by the power supply voltages. The gain saturation is indicated by the reduced transmission peaks and the increased linewidths at higher input power (Fig. 2d,e). Similar to optical systems[23,25,40,41], this saturation nonlinearity breaks the time-reversal symmetry for SAWs, but not the dynamic reciprocity[42]. Meanwhile, SAW loss is implemented by an IDT connected to a resistor, and it behaves linearly within our range of input powers (Supplementary Fig. 9).

Our PT-symmetric SAW devices can operate in the unbroken or broken symmetry regimes by adjusting the coupling strength, gain or loss of the resonators (Supplementary Note 2). The coupling strength is experimentally controlled by varying the number of Bragg mirror grooves between the two resonators and varies from $\mu = 295$ kHz for 20 grooves to $\mu = 9$ kHz for 90 grooves (Supplementary Fig. 11). An 80-groove mirror ($\mu = 27$ kHz) is used for measurements in the non-reciprocal broken PT-symmetric regime, while a 30-groove mirror ($\mu = 180$ kHz) is used for the reciprocal unbroken PT-symmetric regime.

Measurements of non-reciprocal transmission

The SAW devices and electronic circuits were assembled on a printed circuit board for transmission measurements (Extended Data Fig. 1). Non-reciprocal transmission is observed in the broken PT-symmetric regime (Fig. 3a), in which the loss and gain of the resonators are tuned to maximize the non-reciprocal isolation. At the optimum input power of 3 μW (−25 dBm), a Lorentzian resonance peak is observed in the forward transmission spectrum, while a reduced transmission near the SAW resonance frequency is observed in the backward transmission spectrum. A non-reciprocity of $\eta = 10.9$ dB is calculated from

$$\eta = \left.\frac{S_{\mathrm{Fwd}}(f_0)}{S_{\mathrm{Bwd}}(f_0)}\right|_{S_{\mathrm{Fwd}}(f_0)=\max(S_{\mathrm{Fwd}})} \quad (1)$$

where $S_{\mathrm{Fwd}}(f)$ and $S_{\mathrm{Bwd}}(f)$ are the power transmission coefficients in the forward and backward directions, respectively, and frequency f_0 corresponds to the maximum forward transmission. The forward and backward transmission spectra are measured separately by launching a SAW from one input at a time. The measured maximum forward power transmission of $S_{\mathrm{Fwd}} = 0.2$ corresponds to an insertion loss of 7 dB. The full-width at half-maximum bandwidth of the forward input is measured to be 28 kHz, which is consistent with the linewidth of the active SAW resonator. The non-reciprocity varies with power because the nonlinearity is induced by saturation (Extended Data Fig. 2). The dynamic range of the input SAW, which is defined by a 3 dB degradation of non-reciprocity, is measured to be 8 dB, ranging from −28 dBm (1.6 μW) to −20 dBm (10 μW). At a lower input power of 250 nW, SAWs propagating in both directions experience linear gain, and thus no significant non-reciprocity, while at a high input power of 40 μW, the non-reciprocity is reduced because SAWs propagating in both directions experience strong nonlinear saturation.

Our experiments clarify that the non-reciprocity of the nonlinear PT system originates from the inequality of nonlinear gains induced by PT symmetry breaking for the forward and backward inputs, and eliminate the confusion about the origin of non-reciprocity in optical PT-symmetric systems[23], in which full control and direct observation of nonlinearity are not available. Furthermore, the desired SAW transmission in the forward direction can be linear and free from nonlinear distortion. Under the optimal input power of 3 μW, our PT-symmetric system remains in the linear regime for forward-propagating signals. However, for backward-propagating signals, stronger localization in the active resonator triggers strong nonlinear saturation and suppresses the transmission. We use the relative powers at higher harmonics to characterize the nonlinearity of the transmitted signals (Supplementary Fig. 12). For forward transmission, the power ratio of the second harmonic is only −31 dBc (0.08%) at the optimal input power. For backward transmission, at the same input power, the power ratio of the second harmonic is as high as −13 dBc (5%).

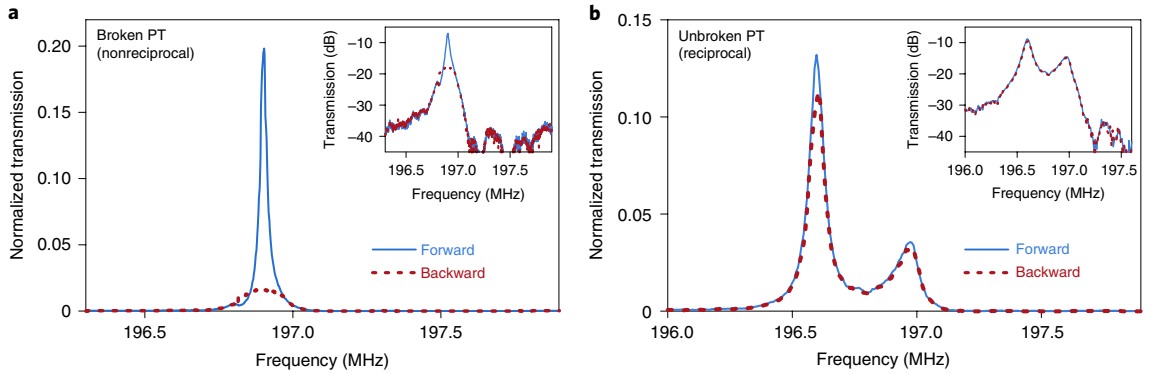

Fig. 3 | SAW transmission of the nonlinear PT-symmetric resonators. a, Non-reciprocal transmission measurements of the SAW resonators in the broken PT-symmetric regime. **b**, Reciprocal transmission measurements of the SAW resonators in the unbroken PT-symmetric regime. The microwave power applied to the input IDTs is −25 dBm (3 μW) in both plots. Insets: transmission plotted on a logarithmic scale. The transmission is normalized to that of a pair of IDTs.

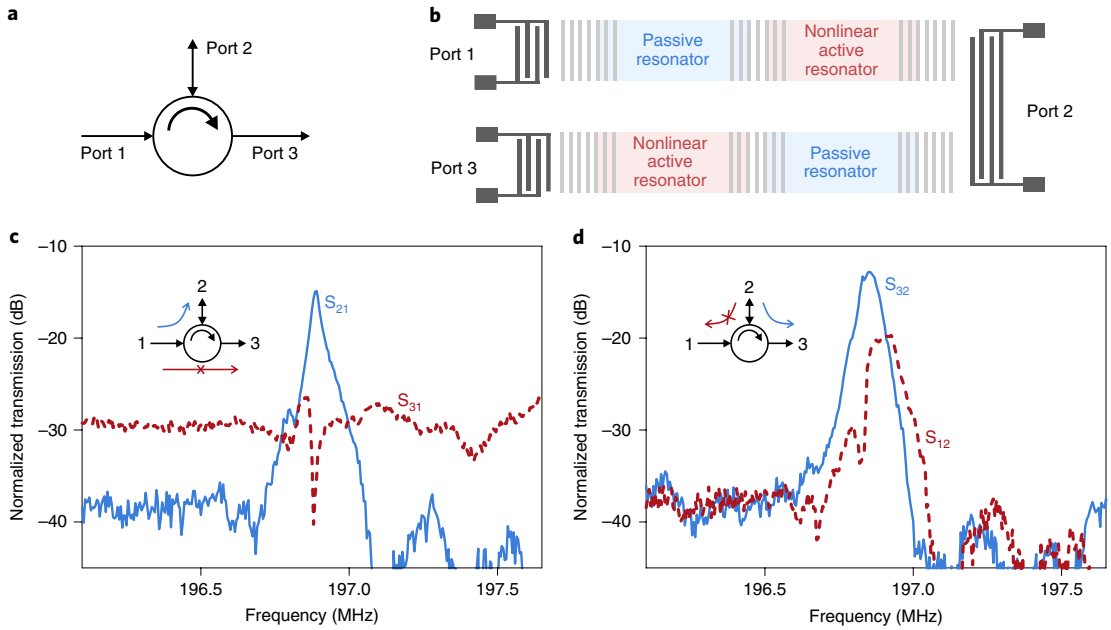

Fig. 4 | One-way circulation of SAWs. a, Illustration of circulation that allows transmission in the clockwise direction (that is, from port 1 to port 2, port 2 to port 3) and blocks transmission in the counterclockwise direction (that is, from port 2 to port 1, port 3 to port 2). **b**, Schematic of the SAW circulation with two non-reciprocal devices connected in series. **c**,**d**, Transmission measurements between different ports, as shown in the insets in **c** and **d**. The transmission is normalized to that of a pair of IDTs.

In contrast, reciprocal transmission is observed in the unbroken PT-symmetric regime (Fig. 3b) using the resonator with a 30-groove mirror (coupling strength of $\mu = 180$ kHz) and the same nonlinear gain and loss circuit. At the same input power of 3 μW, similar transmission spectra with split resonances are observed for both forward and backward SAW inputs. Although saturation nonlinearity is observed with increasing input powers in both transmission directions, only reciprocal transmission is observed in this unbroken regime.

The concept of non-reciprocal SAW transmission can be leveraged in many applications. As an example, we demonstrate the one-way circulation of SAWs using two non-reciprocal devices (Fig. 4a,b). Circulation is observed at the resonance frequency of the device. A SAW from port 1 is almost entirely transmitted to port 2 (S_{21}). At the frequency of the maximum transmission in the S_{21} spectrum, transmission in the clockwise direction S_{21} is 20 dB higher than that in the counterclockwise direction S_{31} (Fig. 4c). Similarly, for a SAW from port 2, the transmission to port 3 is 10 dB higher than that to port 1 (Fig. 4d). The higher off-resonance transmission between port 3 and port 1 is caused by electrical crosstalk due to the proximity of the IDTs. The discrepancy between different input ports is probably caused by the small variation in resonance frequencies and Q factors of the acoustic resonators.

Performance of the non-reciprocal SAW devices

The performance of our non-reciprocal SAW devices is not fundamentally limited and could be improved. We evaluated the dependence of the non-reciprocity, the dynamic range and the insertion on the device parameters, including the coupling strengths and the gain in Supplementary Note 3. From the theoretical analysis, a non-reciprocity of over 35 dB, a dynamic range of over 50 dB and an insertion loss of 0 dB could each be feasible with our non-reciprocal

SAW resonators. However, there is a trade-off between the various parameters. Generally, a weaker coupling strength between the SAW resonators leads to a larger dynamic range, but greater insertion loss, while higher gain of the active resonator will result in stronger non-reciprocity, lower insertion loss, but a smaller dynamic range. In practice, the gain and nonlinearity are limited by the commercially available operational amplifiers used in our demonstration, which are not designed to have strong nonlinearities. An integrated circuit designed specifically for this purpose or a nonlinear superconducting circuit could further improve the non-reciprocity of our SAW devices. We note that use of the gain would inevitably bring noise into the system. However, passive PT-symmetric acoustic systems could be constructed to avoid the additional noise due to the gain, as has been demonstrated for optical systems[27–29].

Conclusions

We have reported a compact piezoelectric platform based on lithium niobate for non-Hermitian and non-reciprocal acoustic wave propagation. The electrically tuned gain and loss of two coupled acoustic resonators introduce nonlinearity, breaking the PT symmetry of the system. In our experiments, we used acoustic waves with an operating frequency of 200 MHz, but the frequency could be extended to a few gigahertz by geometrically scaling the design[39]. Furthermore, a fully integrated high-frequency acoustic platform could also be built using application-specific integrated circuits, instead of discrete electronic components. Our PT-symmetric system could be of use in the manipulation, routing and amplification of microwave phonons in integrated devices, and our active SAW circuits could enrich acoustic signal processing for next-generation wireless communication.

Methods

Device design and fabrication. The SAW devices were fabricated on a 128° Y-cut $LiNbO_3$ substrate (the SAW propagates in the X direction of the crystal). The SAW resonators were defined by Bragg mirrors (periodically etched grooves). The length of a single SAW resonator was 600 μm (between the edges of the Bragg mirrors). The grooves were patterned by photolithography using a maskless aligner (Heidelberg Instruments MLA 150), and the $LiNbO_3$ was etched by reactive-ion etching using argon gas. The pitch of the grooves was 10 μm (which matches the half-wavelength of the SAW for a frequency of ~197 MHz) and the etch depth was 0.5 μm. The width of the grooves was 5 μm at the centre of the Bragg mirror and tapered to zero within 10 periods at both ends of the Bragg mirror to reduce acoustic losses (Fig. 1b). The number of grooves for the external Bragg mirror was 54, while the number of grooves for the coupling Bragg mirror, which determines the coupling strength between two resonators, varied from 20 to 90 for strongly coupled to weakly coupled resonators. IDTs, electrical connections and contact pads were fabricated using 120-nm-thick aluminium deposited by thermal evaporation and patterned by photolithography and a liftoff process. The electrode pitch (width) of the IDT was 9.8 μm (4.9 μm) and its central frequency matched the SAW resonance frequency. The presence of the metal reduced the speed of the SAW, and the pitch of the IDT was thus slightly smaller than the pitch of the groove. The number of electrodes was 38 (19 signal and 19 ground electrodes) for the external IDTs outside the SAW resonators. These IDTs gave a bandwidth of ~10 MHz from the transmission measurements and covered the reflection band of the Bragg mirror. For the in-resonator IDTs that provide SAW loss and gain, the number of electrodes was 8 (4 signal and 4 ground electrodes). The contact pads were wire-bonded to the printed circuit board (Extended Data Fig. 1).

Data availability

Source data are available for the graphs plotted in Figs. 1–4 and Extended Data Fig. 2. All other data and findings of this study are available from the corresponding author upon reasonable request.

Received: 30 September 2019; Accepted: 16 April 2020;
Published online: 18 May 2020

References

1. Chu, Y. et al. Quantum acoustics with superconducting qubits. *Science* **358**, 199–202 (2017).
2. Satzinger, K. J. et al. Quantum control of surface acoustic-wave phonons. *Nature* **563**, 661–665 (2018).
3. Whiteley, S. J. et al. Spin–phonon interactions in silicon carbide addressed by Gaussian acoustics. *Nat. Phys.* **15**, 490–495 (2019).
4. Maity, S. et al. Coherent acoustic control of a single silicon vacancy spin in diamond. *Nat. Commun.* **11**, 193 (2020).
5. Arrangoiz-Arriola, P. et al. Resolving the energy levels of a nanomechanical oscillator. *Nature* **571**, 537–540 (2019).
6. Otterstrom, N. T., Behunin, R. O., Kittlaus, E. A., Wang, Z. & Rakich, P. T. A silicon Brillouin laser. *Science* **360**, 1113–1116 (2018).
7. Campbell, C. *Surface Acoustic Wave Devices and their Signal Processing Applications* (Academic Press, 1989).
8. Fleury, R., Sounas, D. L., Sieck, C. F., Haberman, M. R. & Alù, A. Sound isolation and giant linear nonreciprocity in a compact acoustic circulator. *Science* **343**, 516–519 (2014).
9. Liang, B., Guo, X. S., Tu, J., Zhang, D. & Cheng, J. C. An acoustic rectifier. *Nat. Mater.* **9**, 989–992 (2010).
10. Liang, B., Yuan, B. & Cheng, J. C. Acoustic diode: rectification of acoustic energy flux in one-dimensional systems. *Phys. Rev. Lett.* **103**, 104301 (2009).
11. Li, Y. et al. Tunable asymmetric transmission via lossy acoustic metasurfaces. *Phys. Rev. Lett.* **119**, 035501 (2017).
12. Popa, B. I. & Cummer, S. A. Non-reciprocal and highly nonlinear active acoustic metamaterials. *Nat. Commun.* **5**, 3398 (2014).
13. Walker, E. et al. Nonreciprocal linear transmission of sound in a viscous environment with broken *P* symmetry. *Phys. Rev. Lett.* **120**, 204501 (2018).
14. Devaux, T., Cebrecos, A., Richoux, O., Pagneux, V. & Tournat, V. Acoustic radiation pressure for nonreciprocal transmission and switch effects. *Nat. Commun.* **10**, 3292 (2019).
15. Sasaki, R., Nii, Y., Iguchi, Y. & Onose, Y. Nonreciprocal propagation of surface acoustic wave in $Ni/LiNbO_3$. *Phys. Rev. B* **95**, 020407 (2017).
16. Nomura, T. et al. Phonon magnetochiral effect. *Phys. Rev. Lett.* **122**, 145901 (2019).
17. Xu, H., Jiang, L., Clerk, A. A. & Harris, J. G. E. Nonreciprocal control and cooling of phonon modes in an optomechanical system. *Nature* **568**, 65–69 (2019).
18. Bender, C. M. & Boettcher, S. Real spectra in non-Hermitian Hamiltonians having PT symmetry. *Phys. Rev. Lett.* **80**, 5243–5246 (1998).
19. El-Ganainy, R. et al. Non-Hermitian physics and PT symmetry. *Nat. Phys.* **14**, 11–19 (2018).
20. Konotop, V. V., Yang, J. & Zezyulin, D. A. Nonlinear waves in PT-symmetric systems. *Rev. Mod. Phys.* **88**, 035002 (2016).
21. Li, Y. et al. Anti-parity–time symmetry in diffusive systems. *Science* **364**, 170–173 (2019).
22. Feng, L., El-Ganainy, R. & Ge, L. Non-Hermitian photonics based on parity–time symmetry. *Nat. Photon.* **11**, 752–762 (2017).
23. Peng, B. et al. Parity–time-symmetric whispering-gallery microcavities. *Nat. Phys.* **10**, 394–398 (2014).
24. Feng, L. et al. Experimental demonstration of a unidirectional reflectionless parity–time metamaterial at optical frequencies. *Nat. Mater.* **12**, 108–113 (2013).
25. Chang, L. et al. Parity–time symmetry and variable optical isolation in active–passive-coupled microresonators. *Nat. Photon.* **8**, 524–529 (2014).
26. Feng, L., Wong, Z. J., Ma, R.-M., Wang, Y. & Zhang, X. Single-mode laser by parity–time symmetry breaking. *Science* **346**, 972–975 (2014).
27. Klauck, F. et al. Observation of PT-symmetric quantum interference. *Nat. Photon.* **13**, 883–887 (2019).
28. Zhen, B. et al. Spawning rings of exceptional points out of Dirac cones. *Nature* **525**, 354–358 (2015).
29. Özdemir, Ş. K., Rotter, S., Nori, F. & Yang, L. Parity–time symmetry and exceptional points in photonics. *Nat. Mater.* **18**, 783–798 (2019).
30. Fleury, R., Sounas, D. & Alu, A. An invisible acoustic sensor based on parity–time symmetry. *Nat. Commun.* **6**, 5905 (2015).
31. Shi, C. et al. Accessing the exceptional points of parity–time symmetric acoustics. *Nat. Commun.* **7**, 11110 (2016).
32. Auregan, Y. & Pagneux, V. PT-symmetric scattering in flow duct acoustics. *Phys. Rev. Lett.* **118**, 174301 (2017).
33. Zhu, X., Ramezani, H., Shi, C., Zhu, J. & Zhang, X. PT-symmetric acoustics. *Phys. Rev. X* **4**, 031042 (2014).
34. Zhang, J. et al. Giant nonlinearity via breaking parity–time symmetry: a route to low-threshold phonon diodes. *Phys. Rev. B* **92**, 115407 (2015).
35. Xu, X.-W., Liu, Y.-x, Sun, C.-P. & Li, Y. Mechanical PT symmetry in coupled optomechanical systems. *Phys. Rev. A* **92**, 013852 (2015).
36. Bender, C. M., Berntson, B. K., Parker, D. & Samuel, E. Observation of PT phase transition in a simple mechanical system. *Am. J. Phys.* **81**, 173–179 (2013).
37. Assawaworrarit, S., Yu, X. & Fan, S. Robust wireless power transfer using a nonlinear parity–time-symmetric circuit. *Nature* **546**, 387–390 (2017).
38. Morgan, D. & Paige, E. G. S. *Surface Acoustic Wave Filters with Applications to Electronic Communications and Signal Processing* (Academic Press, 2007).
39. Shao, L. et al. Phononic band structure engineering for high-Q gigahertz surface acoustic wave resonators on lithium niobate. *Phys. Rev. Appl.* **12**, 014022 (2019).

40. Jiang, X. et al. On-chip optical nonreciprocity using an active microcavity. *Sci. Rep.* **6**, 38972 (2016).
41. Wen, J. et al. Modeling of on-chip optical nonreciprocity with an active microcavity. *Photonics* **2**, 498–508 (2015).
42. Shi, Y., Yu, Z. & Fan, S. Limitations of nonlinear optical isolators due to dynamic reciprocity. *Nat. Photon.* **9**, 388–392 (2015).

Acknowledgements

We thank S. Bogdanovic, M. Yu, M. Zhang, C. Chia, B. Machielse and Y.-F. Xiao for fruitful discussions. This work is supported by the STC Center for Integrated Quantum Materials, NSF grant no. DMR-1231319, NSF CQIS grant no. ECCS-1810233, ONR MURI grant no. N00014-15-1-2761 and AFOSR MURI grant no. FA9550-14-1-0389. N.S. acknowledges support by the Natural Sciences and Engineering Research Council of Canada (NSERC), the AQT Intelligent Quantum Networks and Technologies (INQNET) research programme and the DOE/HEP QuantISED programme grant and QCCFP (Quantum Communication Channels for Fundamental Physics) award no. DE-SC0019219. W.M. acknowledges support from the undergraduate overseas internship programme of Nankai University supported by the National Science Fund for Talent Training in the Basic Sciences, grant no. J1103208. This work was performed in part at the Center for Nanoscale Systems (CNS), Harvard University.

Author contributions

L.S. conceptualized, designed, fabricated and measured the devices. W.M. and Y.H. analysed the system theoretically, with discussion from other authors. W.M. and L.S. performed numerical simulations. All authors analysed and interpreted the results. L.S. and W.M. prepared the manuscript with contributions from all authors. M.L. and L.Y. supervised the project.

Competing interests

M.L. is involved in developing lithium niobate technologies at HyperLight Corporation. The other authors declare no competing interests.

Additional information

Supplementary information is available for this paper at https://doi.org/10.1038/s41928-020-0414-z.

Correspondence and requests for materials should be addressed to L.S. or M.L.

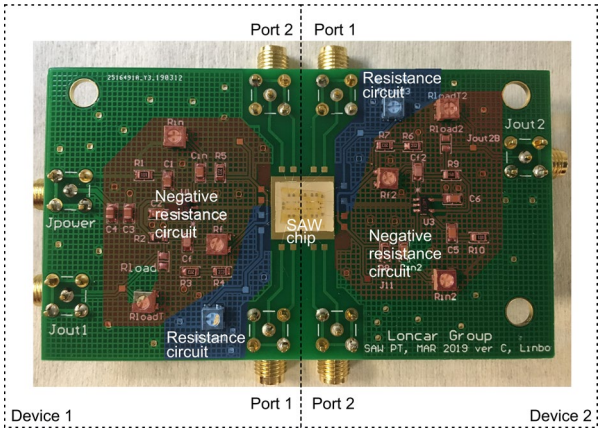

Extended Data Fig. 1 | Photo of the printed circuit board (PCB) used for non-reciprocal SAW device measurements. This PCB supports simultaneous measurements of two devices. Signal from Port 1 to Port 2 is defined as the forward direction.

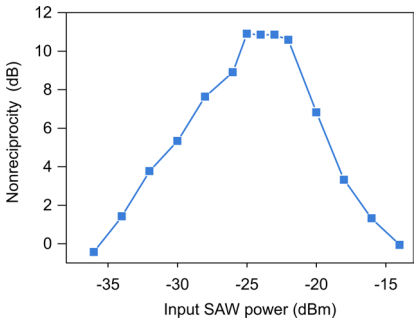

Extended Data Fig. 2 | Measured non-reciprocity of the broken-PT-symmetric SAW resonators versus various input powers. The non-reciprocity is defined in Equ. (1).

Terms and Conditions

Springer Nature journal content, brought to you courtesy of Springer Nature Customer Service Center GmbH (“Springer Nature”).
Springer Nature supports a reasonable amount of sharing of research papers by authors, subscribers and authorised users (“Users”), for small-scale personal, non-commercial use provided that all copyright, trade and service marks and other proprietary notices are maintained. By accessing, sharing, receiving or otherwise using the Springer Nature journal content you agree to these terms of use (“Terms”). For these purposes, Springer Nature considers academic use (by researchers and students) to be non-commercial.
These Terms are supplementary and will apply in addition to any applicable website terms and conditions, a relevant site licence or a personal subscription. These Terms will prevail over any conflict or ambiguity with regards to the relevant terms, a site licence or a personal subscription (to the extent of the conflict or ambiguity only). For Creative Commons-licensed articles, the terms of the Creative Commons license used will apply.
We collect and use personal data to provide access to the Springer Nature journal content. We may also use these personal data internally within ResearchGate and Springer Nature and as agreed share it, in an anonymised way, for purposes of tracking, analysis and reporting. We will not otherwise disclose your personal data outside the ResearchGate or the Springer Nature group of companies unless we have your permission as detailed in the Privacy Policy.
While Users may use the Springer Nature journal content for small scale, personal non-commercial use, it is important to note that Users may not:

1. use such content for the purpose of providing other users with access on a regular or large scale basis or as a means to circumvent access control;
2. use such content where to do so would be considered a criminal or statutory offence in any jurisdiction, or gives rise to civil liability, or is otherwise unlawful;
3. falsely or misleadingly imply or suggest endorsement, approval , sponsorship, or association unless explicitly agreed to by Springer Nature in writing;
4. use bots or other automated methods to access the content or redirect messages
5. override any security feature or exclusionary protocol; or
6. share the content in order to create substitute for Springer Nature products or services or a systematic database of Springer Nature journal content.

In line with the restriction against commercial use, Springer Nature does not permit the creation of a product or service that creates revenue, royalties, rent or income from our content or its inclusion as part of a paid for service or for other commercial gain. Springer Nature journal content cannot be used for inter-library loans and librarians may not upload Springer Nature journal content on a large scale into their, or any other, institutional repository.
These terms of use are reviewed regularly and may be amended at any time. Springer Nature is not obligated to publish any information or content on this website and may remove it or features or functionality at our sole discretion, at any time with or without notice. Springer Nature may revoke this licence to you at any time and remove access to any copies of the Springer Nature journal content which have been saved.
To the fullest extent permitted by law, Springer Nature makes no warranties, representations or guarantees to Users, either express or implied with respect to the Springer nature journal content and all parties disclaim and waive any implied warranties or warranties imposed by law, including merchantability or fitness for any particular purpose.
Please note that these rights do not automatically extend to content, data or other material published by Springer Nature that may be licensed from third parties.
If you would like to use or distribute our Springer Nature journal content to a wider audience or on a regular basis or in any other manner not expressly permitted by these Terms, please contact Springer Nature at

onlineservice@springernature.com